International Journal of Advanced Robotic Systems

OPEN ACCESS
ARTICLE

Formation Tracking Based on Approximate Velocities

Regular Paper

Eduardo Gamaliel Hernandez-Martinez[1]*, Jose-Job Flores-Godoy[2], Guillermo Fernandez-Anaya[3] and Alexandro Lopez-Gonzalez[1]

1 Departamento de Ingenierías, Universidad Iberoamericana, Mexico City, Mexico
2 Departamento de Matemática, Universidad Catolica del Uruguay, Montevideo, Uruguay
3 Departamento de Física y Matemáticas, Universidad Iberoamericana, Mexico City, Mexico
*Corresponding author(s) E-mail: eduardo.gamaliel@ibero.mx

Received 04 March 2015; Accepted 04 November 2015

DOI: 10.5772/61944

Abstract

This paper analyses the formation tracking of groups of mobile robots moving on the plane. A leader robot is chosen to follow a prescribed trajectory whilst the rest, considered as followers, are formed in an open-chain configuration. Two formation-tracking control laws using approximate velocities are proposed, in which some velocities must be communicated between robots in order to ensure the simultaneous preservation of the formation and the following of the group path. The main result is analysis of the convergence of the two proposed control laws. The restriction of inaccurate information occurs in decentralized multi-robot platforms, in which the mobile agents are only able to measure positions and the velocities' functions are estimated using online numerical methods. A numerical simulation of both controllers in the case of omnidirectional robots is shown. For the case of the unicycle-type robots, real-time experiments of both controllers were implemented and tested.

Keywords Formation Control, Marching Control, Multi-robot Systems, Autonomous Robots

1. Introduction

Recently, the motion coordination of multiple biological entities has inspired the design and implementation of natural behaviours in mobile robots for industrial and service applications [1, 2]. Observations of ethologists have determined that the ordered motion of ants, fishes or birds is constructed from local interactions between mobile agents. Each agent acts according to the local information acquired from other members [3]. Therefore, the control schemes are decentralized and the study falls within the research areas of multi-agent systems, sensor networks and distributed control systems. The decentralized schemes also permit more autonomy for the robots, a smaller computational load in control implementations and the method's applicability to large-scale groups [4].

A special case of motion coordination is formation tracking [4, 5], also called marching control [6] or flocking behaviour [7], in which a group of mobile robots achieves geometric patterns whilst the whole group follows a prescribed marching trajectory. Formation tracking appears in some applications such as the transportation and manipulation of large objects, search and rescue tasks and perimeter detection, etc. In formation tracking, it is required that the

group follows some trajectories in the workspace, while a rigid formation pattern is preserved simultaneously. Thus, the main challenge of formation tracking is the inter-robot strategic sharing of information about the marching path or the velocities of certain robots in the group, in order to ensure the formation's preservation, maintaining the greatest possible level of decentralization.

The leader-follower schemes [8, 9] are frequently studied by the academic community due to the inspiration that biological behaviour creates (for instance, in ants). In these schemes, a unique leader robot follows a marching path while the rest, termed followers, converge to some formation pattern with respect to the leader. Although some contributions have been proposed in relation to formation tracking, most of the studies consider that the robots can measure the exact information about the velocities of the other robots or the marching path. For instance, [10] studies the case of a convoy-like formation, in which the robots are initially placed at the desired positions, and they know the linear and angular velocities of the adjacent robot. The positions and orientations of virtual leaders serve as reference points for the follower robots in [11, 12] and the exact marching path derivative is available to all robots in [6, 5].

Note that in the natural leader-followers scheme, each agent is able to sense the position of only the nearby agents, and the velocities must be estimated or intuited by their local controllers. As will be discussed below, if some velocities are not approximated in the control laws, then the formation is not rigid during the path following, as shown in [13, 14], in which the positions of the followers vary in a ball that is centred in terms of the leader's reference frame. Some papers estimated the leader's velocity using position measurements acquired through observers [15] or local sensors [16]. The problem of formation tracking is studied via an estimator designed to track a globally desired velocity that is available to a subset of robots via a consensus-based velocity term in [17]. Predictive control is applied in [18], which added a term to the cost function of the leader in order to preserve the formation. Other works focus on the reconstruction of the marching path using adaptive algorithms in [19, 20, 21, 22], and Lyapunov techniques in [23]. The velocities of neighbours are estimated in [24, 25] in order to construct the desired marching path based on local information. Recently, the approximation of velocities for the case of spacecraft formations was obtained by using a non-linear filter with finite-time convergence in [26]. Most previous works designed estimation methods for the velocity of the agents based on the measurement of the marching path's exact velocity, decreasing decentralization and simplicity of the control laws. Commonly, some numerical methods are included in order to estimate velocities in the experimental platforms of multi-robot systems. However, the effects of these approximations have not been formally analysed.

In [27], two formation-tracking control laws were designed using exact velocity measurements in order to achieve formation-tracking convergence. This paper shows the boundedness of the formation-tracking error when only position information is used. The variation of the formation-tracking error can be made arbitrarily small when the approximations of velocities are close to the real values. In addition, for a class of tracking trajectory, we show the exponential convergence of the formation-tracking error. This study is important, since this is the way that such implementation is usually done. Nevertheless, the degradation of the performance on the overall system has not been formally studied. To show the effects of the approximate velocities, the control laws were extended to unicycle-type robots in real-time experiments.

The rest of the paper is organized as follows. Section 2 introduces the kinematic model and the problem statement. A short summary of our previous formation-tracking control strategy, with its exact velocities, is presented in Section 3 with numerical simulations. The main result of the paper is given in Section 4, using approximate velocities with numerical simulations. The extension of the model to unicycle-type robots and the real-time experiments are shown in Sections 5 and 6, respectively. Finally, some concluding remarks are presented in Section 7.

2. Problem Definition

Denote by $N=\{R_1,...,R_n\}$, a set of n point robots moving in the space with positions $z_i(t)=[x_i(t),y_i(t)]^T$, $i=1,...,n$. The kinematic model of each agent or robot R_i is described by

$$\dot{z}_i = u_i, i = 1,...,n, \tag{1}$$

where $u_i \in \Re^2$ is the velocity along the X and Y axes of the i -th robot. Let $R_1,...,R_{n-1}$ be the follower robots, and R_n be the leader robot. Based on the leader-follower scheme, define z_i^* as the desired relative position of R_i in a particular formation, given by

$$\begin{aligned} z_i^* &= z_{i+1} + c_{(i+1)i}, \quad i = 1,...,n-1, \\ z_n^* &= m(t), \end{aligned} \tag{2}$$

where $c_{(i+1)i} \in \Re^2$, $i=1,...,n-1$ denotes the vector that represents the desired relative position of R_i with respect to R_{i+1} and $m(t)=[m_x(t),m_y(t)] \in \Re^2$ is the marching path (a twice-differentiable function) of the leader.

Remark 1 *Note that the variables z_i, $i=1,...,n$ are the absolute position vectors of the robots with respect to the global reference frame. Therefore, the variables z_i^*, $i=1,...,n$ given in (2) are also absolute coordinates. However, in the context of formation control, z_i^*, $i=1,...,n$ are called desired relative positions in the sense that they depend on the positions of other robots. Therefore,*

the word relative does not indicate that z_i^*, $i=1,...,n$ are measured with respect to a different reference frame.

Figure 1 shows an example of formation tracking in which the robots satisfy a specific formation pattern while simultaneously following the trajectory $m(t)$. The goal of the leader is to follow the marching path, whereas the goal of the followers is to maintain a desired pattern formation with respect to the leader, using the position of the adjacent robot as a guide. This strategy is usually considered as an open-chain or convoy configuration [10]. Note that the marching path could be constructed online by a human operator, who controls the displacement of the leader remotely while the followers achieve a formation.

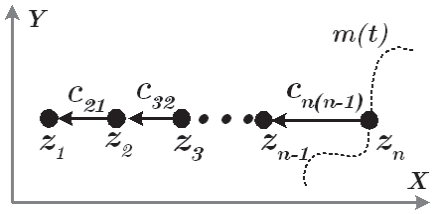

Figure 1. Desired formation tracking of the robots

Problem Statement. The goal of formation tracking is to design a control law $u_i = f_i(z_i, z_i^*)$ for every robot R_i, such that $\lim_{t\to\infty}(z_i - z_i^*)=0$, $i=1,...,n$.

3. Control strategy based on the exact information of velocities

Based on [27], for every follower robot, Local Potential Functions (LPFs) are defined by

$$\gamma_i = \| z_i - z_i^* \|^2, i = 1,...,n-1 \tag{3}$$

Note that γ_i is always positive and reaches its minimum only when $z_i = z_i^*$. The standard approach of (attractive) LPFs consists in applying the partial derivative of an LPF with respect to z_i, as control inputs of every robot R_i. Thus, the control inputs steer every robot to achieve the minimum of this potential function, which is designed according to the specific position vectors that construct a particular formation. Using these functions, two control laws can be defined by

$$\Gamma_1 : \begin{cases} u_i = -\frac{1}{2}k\frac{\partial \gamma_i}{\partial z_i} + \dot{m}(t), \ i = 1,...,n-1 \\ u_n = \dot{m}(t) - k_m\left(z_n - m(t)\right) \end{cases} \tag{4}$$

$$\Gamma_2 : \begin{cases} u_i = -\frac{1}{2}k\frac{\partial \gamma_i}{\partial z_i} + \dot{z}_{i+1}, \ i = 1,...,n-1 \\ u_n = \dot{m}(t) - k_m\left(z_n - m(t)\right) \end{cases} \tag{5}$$

where $k, k_m > 0$. Note that the control law Γ_1 requires the provision of feedback $\dot{m}(t)$ to all followers, and that Γ_2 includes the feedback of the adjacent robot $\dot{z}_{i+1}$ for all followers. Thus, the first $n-1$ robots are not required to process complete information about $m(t)$ or the positions of all robots, unlike in [4] or [28], in which all robots must know the target position or trajectory, and more than one desired distance between robots. A schematic description of the control strategies is shown in Fig. 3. Observe that the control law of the leader requires the exact derivative of $m(t)$ to function, whilst the followers require the full knowledge of $\dot{m}(t)$ or $\dot{z}_{i+1}$.

With respect to the convergence of the desired formation tracking using (4) or (5), the next proposition can be found in [27].

Proposition 1 *Consider the system (1) and the control laws (4) or (5) for n robots. Then, in the closed-loop systems (1), (4) and (1), (5), the first $n-1$ robots converge to the desired formation, i.e., $\lim_{t\to\infty}(z_i - z_i^*)=0$, $i=1,...,n-1$, whereas R_n converges to the marching path, i.e., $\lim_{t\to\infty}(z_n(t) - m(t))=0$.*

A sketch of the proof is included for completeness.

Proof. The dynamics of z_i in the closed-loop systems (1), (4) and (1), (5) are given, respectively, by

$$(1),(14) : \begin{cases} \dot{z}_i = -k\left(z_i - z_{i+1} - c_{(i+1)i}\right) + \dot{m}(t), \\ i = 1,...,n-1 \\ \dot{z}_n = \dot{m}(t) - k_m\left(z_n - m(t)\right) \end{cases} \tag{6}$$

$$(141),(1415) : \begin{cases} \dot{z}_i = -k\left(z_i - z_{i+1} - c_{(i+1)i}\right) + \dot{z}_{i+1}, \\ i = 1,...,n-1 \\ \dot{z}_n = \dot{m}(t) - k_m\left(z_n - m(t)\right) \end{cases} \tag{7}$$

Define the error variables by

$$e_i = z_i - z_i^*, i = 1,...,n \tag{8}$$

where $e_1,...,e_{n-1}$ are the formation errors of the followers and e_n is the path-following error of the leader. The dynamics of the error coordinates (8) for the two control laws are given respectively by

$$\dot{e} = \left(B_1 \otimes I_2\right)e \tag{9}$$

$$\dot{e} = \left(B_2 \otimes I_2\right)e \tag{10}$$

where $\otimes$ denotes the Kronecker product (the Kronecker product allows use of a more compact notation for the equations), I_2 is the 2×2 identity matrix and the matrices B_1 and B_2 are

$$B_1 = \begin{bmatrix} -k & k & 0 & 0 & \cdots & 0 & 0 \\ 0 & -k & k & 0 & \cdots & 0 & 0 \\ 0 & 0 & -k & k & \cdots & 0 & 0 \\ 0 & 0 & 0 & \ddots & \ddots & \vdots & 0 \\ \vdots & \vdots & \vdots & \vdots & \ddots & \ddots & \vdots \\ 0 & 0 & 0 & 0 & \cdots & -k & k_m \\ 0 & 0 & 0 & 0 & \cdots & 0 & -k_m \end{bmatrix},$$

$$B_2 = \begin{bmatrix} -k & 0 & 0 & \cdots & 0 & 0 \\ 0 & -k & 0 & \cdots & 0 & 0 \\ \vdots & \vdots & \vdots & \ddots & \vdots & \vdots \\ 0 & 0 & 0 & \cdots & -k & 0 \\ 0 & 0 & 0 & \cdots & 0 & -k_m \end{bmatrix}.$$

Clearly, the matrices B_1 and B_2 are Hurwitz ones, and the errors converge to zero. This means that the $n-1$ first agents converge to the desired formation, whereas R_n converges to the marching path. □

Remark 2 *It is necessary to add $\dot{m}(t)$ in Γ_1 and $\dot{z}_{i+1}$ in Γ_2 in order to guarantee the preservation of the formation during the trajectory tracking. If they are not included, the errors' time derivatives become $\dot{e}=(B_1 \otimes I_2)e+[S_x,S_y]^T$ or $\dot{e}=(B_2 \otimes I_2)e+[S_x,S_y]^T$, with $S_x=[0,...,0,\dot{m}_x(t),0]^T$ and $S_y=[0,...,0,\dot{m}_y(t),0]^T$. Even though the matrices B_1 and B_2 are clearly Hurwitz ones, the dynamics of R_{n-1} is disturbed by the marching velocity and it is transmitted to the other followers. This is an example of disturbance propagation in chain-stability in formation control using the leader-followers' scheme [9], in which the motion of the leader influences the formation stability of the followers.*

The control strategies (4) and (5) are appropriated for any kind of sufficiently smooth function $m(t)$. Figure 3 shows a numerical simulation of both control laws with $n=3$, $k=1$ and $k_m=1$. The initial conditions are given by $z_1(0)=[-1,3]$, $z_2(0)=[2,2]$ and $z_3(0)=[2,5]$. The desired formation is a triangle defined by the vectors $c_{21}=[0,-4]$ and $c_{32}=[-3,2]$, and the marching path is a circular path given by $m(t)=[3+\cos(0.2t),3+\sin(0.2t)]$. Note that the follower robots converge to the desired formation and that the leader robot, z_3 (represented by a green dashed line), converges to the marching path $m(t)$. This is shown through the convergence of the error variables. However, the two control laws present differences in the transitory regime.

The convergence of the errors is reached due to the strong assumption that both the velocities of the robots and the marching path are measured exactly. The requirements of the local controllers that the robots include these velocities can be translated into a greater overhead on the communication between the mobile agents. This is the reason motivating analysis of the impact of the velocities' approximation, which is addressed in the next section.

4. Control strategy using the approximations of velocities

Recalling the inspiration derived from nature, in which the mobile agents are capable of sensing only the position of the robots and the marching path, the two control schemes are now modified according to Fig. 4. The robots are not equipped with velocity sensors, and the control laws given

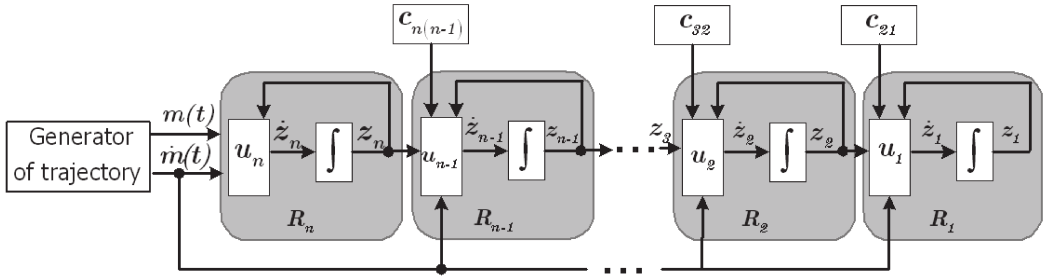

(a) Formation tracking scheme with the control law Γ_1.

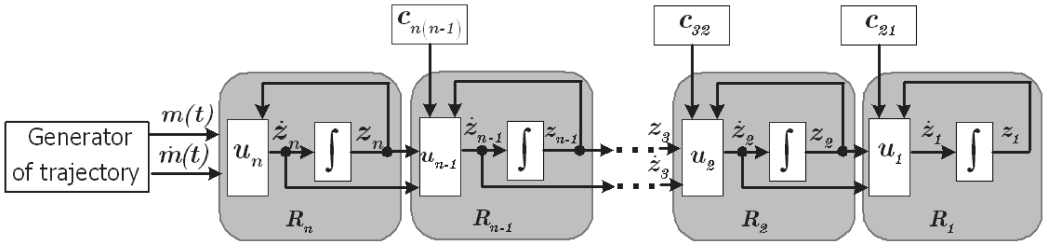

(b) Formation tracking scheme with the control law Γ_2.

Figure 2. Formation-tracking scheme with the exact information about the velocities of robots and the trajectory

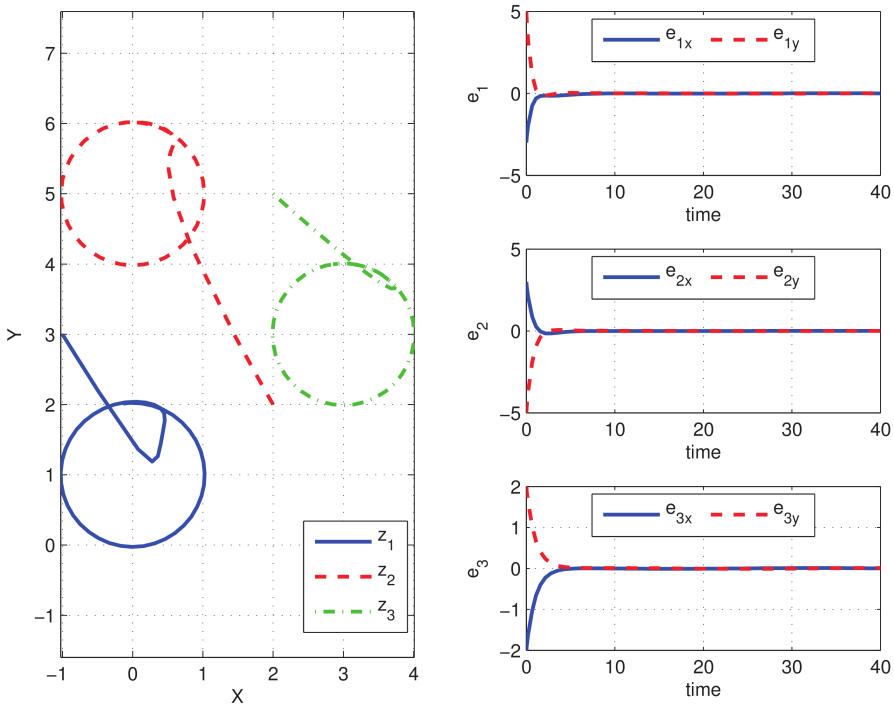

(a) Numerical simulation with the control law Γ_1.

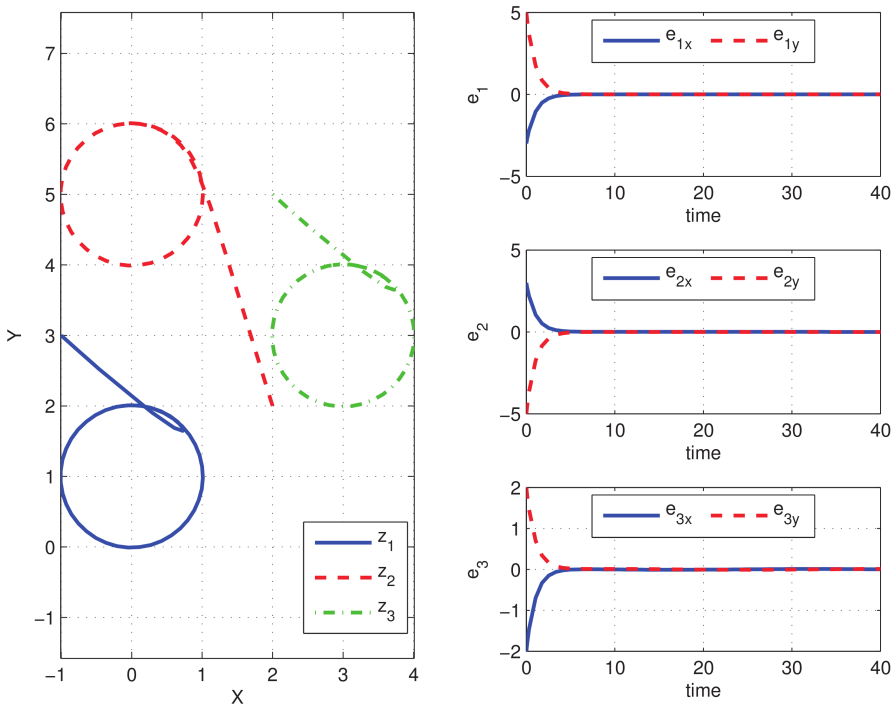

(b) Numerical simulation with the control law Γ_2.

Figure 3. Formation-tracking scheme with the exact information of velocities

by the equations (4) and (5) must be modified in order to incorporate some approximation method for estimating these velocities. The impact of these inexact data on the convergence analysis needs to be studied; hence, a modelled description of the approximation of the derivatives in the system's dynamics is included.

Note that the leader robot needs to approximate the derivative of $m(t)$ and that the follower robots also need to approximate the velocity of the marching path (Figure 4 (a)) or the adjacent robot (Figure 4 (b)). In actual implementations, the velocities are calculated by the local controllers using numerical methods, performing a more

realistic and decentralized scheme. The derivative approximation function shown in Fig. 4 is defined in the frequency domain as

$$g(s) = \frac{s}{\tau s + 1} \tag{11}$$

where $\tau \in \Re$ and $\tau \geq 0$. Thus, the approximation of velocity for a robot R_i and the trajectory $m(t)$ is established by

$$\begin{aligned} \varphi_i(s) &= g(s) z_i(s), \; i = 2,...,n \\ \varphi_m(s) &= g(s) m(s) \end{aligned} \tag{12}$$

Substituting (11) in (12), we obtain

$$\begin{aligned} \varphi_i(s) &= \left(\frac{s}{\tau s+1}\right) z_i(s), \; i = 2,...,n \\ &= \left(1 - \frac{\frac{1}{\tau}}{s+\frac{1}{\tau}}\right)\frac{1}{\tau} z_i(s), \; i = 2,...,n \\ &= \frac{1}{\tau} z_i(s) - \frac{1}{\tau}\left(\frac{\frac{1}{\tau}}{s+\frac{1}{\tau}} z_i(s)\right), \; i = 2,...,n \\ \varphi_m(s) &= \left(\frac{s}{\tau s+1}\right) m(s) \\ &= \left(1 - \frac{\frac{1}{\tau}}{s+\frac{1}{\tau}}\right)\frac{1}{\tau} m(s) \\ &= \frac{1}{\tau} m(s) - \frac{1}{\tau}\left(\frac{\frac{1}{\tau}}{s+\frac{1}{\tau}} m(s)\right) \end{aligned} \tag{13}$$

By defining the auxiliary variables

$$\begin{aligned} \eta_i(s) &= \frac{\frac{1}{\tau}}{s+\frac{1}{\tau}} z_i(s), \; i = 2,...,n \\ \eta_m(s) &= \frac{\frac{1}{\tau}}{s+\frac{1}{\tau}} m(s) \end{aligned} \tag{14}$$

it is possible to obtain from (14)

$$\begin{aligned} s\eta_i(s) &= -\frac{1}{\tau}\eta_i(s) + \frac{1}{\tau} z_i(s), \; i = 2,...,n \\ s\eta_m(s) &= -\frac{1}{\tau}\eta_m(s) + \frac{1}{\tau} m(s) \end{aligned} \tag{15}$$

Therefore, by substituting (14) in (13), and using the inverse Laplace transform on (13) and (15), we can obtain the following differential equations

$$\begin{aligned} \varphi_i &= -\frac{1}{\tau}\eta_i + \frac{1}{\tau} z_i, \; i = 2,....,n \\ \dot{\eta}_i &= -\frac{1}{\tau}\eta_i + \frac{1}{\tau} z_i, \; i = 2,....,n \\ \varphi_m &= -\frac{1}{\tau}\eta_m + \frac{1}{\tau} m(t) \\ \dot{\eta}_m &= -\frac{1}{\tau}\eta_m + \frac{1}{\tau} m(t) \end{aligned} \tag{16}$$

Considering the dynamics of the approximate velocities, the control laws Γ_1 and Γ_2 are modified as

$$\bar{\Gamma}_1 : \begin{cases} u_i = -\frac{1}{2} k \frac{\partial \gamma_i}{\partial z_i} + \varphi_m, \;\; i = 1,...,n-1 \\ u_n = \varphi_m - k_m(z_n - m(t)) \end{cases} \tag{17}$$

$$\bar{\Gamma}_2 : \begin{cases} u_i = -\frac{1}{2} k \frac{\partial \gamma_i}{\partial z_i} + \varphi_{i+1}, i = 1,...,n-1 \\ u_n = \varphi_m - k_m(z_n - m(t)) \end{cases} \tag{18}$$

The closed-loop systems (1), (17) and (1), (18) result in the extended system's equations

$$(1),(117) : \begin{cases} \dot{z}_i = -k\left(z_i - z_{i+1} - c_{(i+1)i}\right) \\ \qquad -\frac{1}{\tau}\eta_m + \frac{1}{\tau} m(t), i = 1,...,n-1 \\ \dot{z}_n = -k_m\left(z_n - m(t)\right) \\ \qquad -\frac{1}{\tau}\eta_m + \frac{1}{\tau} m(t) \\ \dot{\eta}_m = -\frac{1}{\tau}\eta_m + \frac{1}{\tau} m(t) \end{cases} \tag{19}$$

$$(1),(118) : \begin{cases} \dot{z}_i = -k\left(z_i - z_{i+1} - c_{(i+1)i}\right) \\ \qquad -\frac{1}{\tau}\eta_{i+1} + \frac{1}{\tau} z_{i+1}, i = 1,...,n-1 \\ \dot{z}_n = -k_m\left(z_n - m(t)\right) \\ \qquad -\frac{1}{\tau}\eta_m + \frac{1}{\tau} m(t) \\ \dot{\eta}_i = -\frac{1}{\tau}\eta_i + \frac{1}{\tau} z_i, i = 2,....,n \\ \dot{\eta}_m = -\frac{1}{\tau}\eta_m + \frac{1}{\tau} m(t) \end{cases} \tag{20}$$

and, when written in matrix form, the closed-loop systems are given, respectively, by

$$\begin{bmatrix} \dot{z} \\ \dot{\eta}_m \end{bmatrix} = (\Lambda \otimes I_2)\begin{bmatrix} z \\ \eta_m \end{bmatrix} + \begin{bmatrix} C_1 \\ \frac{1}{\tau}m(t) \end{bmatrix} \tag{21}$$

$$\begin{bmatrix} \dot{z} \\ \dot{\eta} \end{bmatrix} = (\Upsilon \otimes I_2)\begin{bmatrix} z \\ \eta \end{bmatrix} + \begin{bmatrix} C_2 \\ M \end{bmatrix} \tag{22}$$

where $z=[z_1,...,z_n]^T$, $\eta=[\eta_2,...,\eta_n,\eta_m]^T$, $M=\left[0,...,0,\frac{1}{\tau}m(t)\right]^T$, $\Lambda=\begin{bmatrix} \Lambda_{11} & \Lambda_{12} \\ \Lambda_{21} & -\frac{1}{\tau} \end{bmatrix}$ with the elements

$$\Lambda_{11} = \begin{bmatrix} -k & k & 0 & 0 & \cdots & 0 & 0 \\ 0 & -k & k & 0 & \cdots & 0 & 0 \\ 0 & 0 & -k & k & \cdots & 0 & 0 \\ 0 & 0 & 0 & \ddots & \ddots & \vdots & 0 \\ \vdots & \vdots & \vdots & \vdots & \ddots & \ddots & \vdots \\ 0 & 0 & 0 & 0 & \cdots & -k & k_m \\ 0 & 0 & 0 & 0 & \cdots & 0 & -k_m \end{bmatrix} \in \Re^{n\times n},$$

$$\Lambda_{12} = [0,...,0]^T \in \Re^{n\times 1},$$

$$\Lambda_{21} = [0,...,0] \in \Re^{1\times n},$$

$=\begin{bmatrix} 11 & 12 \\ 21 & 22 \end{bmatrix}$ with elements

$$\Upsilon_{12} = \Upsilon_{22} = diag\left[-\frac{1}{\tau},...,-\frac{1}{\tau}\right] \in \Re^{n\times n}$$

$$\Upsilon_{11} = \begin{bmatrix} -k & \left(k+\frac{1}{\tau}\right) & 0 & \cdots & 0 & 0 \\ 0 & -k & \left(k+\frac{1}{\tau}\right) & \cdots & 0 & 0 \\ \vdots & \vdots & \ddots & \ddots & \vdots & \vdots \\ \vdots & \vdots & \vdots & \ddots & \ddots & \vdots \\ 0 & 0 & 0 & \cdots & -k & \left(k+\frac{1}{\tau}\right) \\ 0 & 0 & 0 & \cdots & 0 & -k_m \end{bmatrix}$$

$$\Upsilon_{21} = \begin{bmatrix} 0 & \frac{1}{\tau} & 0 & \cdots & 0 & 0 \\ 0 & 0 & \frac{1}{\tau} & \cdots & 0 & 0 \\ \vdots & \vdots & \vdots & \ddots & \vdots & \vdots \\ 0 & 0 & 0 & \cdots & 0 & \frac{1}{\tau} \\ 0 & 0 & 0 & \cdots & 0 & 0 \end{bmatrix} \in \Re^{n\times n}$$

and

$$C_1 = \begin{bmatrix} kc_{21} + \frac{1}{\tau}m(t) \\ \vdots \\ kc_{n(n-1)} + \frac{1}{\tau}m(t) \\ \left(k_m + \frac{1}{\tau}\right)m(t) \end{bmatrix}, C_2 = \begin{bmatrix} kc_{21} \\ \vdots \\ kc_{n(n-1)} \\ \left(k_m + \frac{1}{\tau}\right)m(t) \end{bmatrix}.$$

It is clear that, due to inexact information regarding the velocities, the errors converge to a residual set around zero, which depends on the quality of the approximate velocities. Similar to the previous case, it is necessary to analyse the convergence of the robots to the formation tracking. Thus, we define the following auxiliary variables

$$e_i = z_i - z_i^*, i = 1,...,n$$

$$\delta_i = \varphi_i - \varphi_{i+1}, i = 2,...,n-1$$

$$\delta_n = \varphi_n - \varphi_m(t)$$

$$\delta_{n+1} = \varphi_m - \dot{m}(t)$$

where the errors e_i are similar to (8) and the δ_i errors are the difference between the approximate velocities of the robots and the marching path. Note that if the errors e_i converge to zero, the robots achieve the desired formation and the convergence of δ_i ensures that the robots move at the same velocity as that of the marching path, i.e., preserving the formation pattern.

The next proposition is our main result, which establishes the boundedness of the errors around zero, based on small values of τ and the behaviour of the acceleration of the marching path.

Proposition 2 *Consider the system (1) and the control laws (17) or (18) for n robots. Suppose that $k,k_m>0$. Then, in the closed-loop systems (1), (17) and (1), (18), the error coordinates are bounded for any $\tau\geq 0$ and $|\ddot{m}(t)|<\infty$. Furthermore, if $\ddot{m}(t)=0$, then the errors tend exponentially towards zero, regardless of the value of τ, and when $|\ddot{m}(t)|<\infty$ and $\tau\to 0$, the errors also converge to zero as $t\to\infty$.*

Proof. For the closed-loop system (1), (17), the dynamics of the error coordinates is given by

$$\begin{aligned} \dot{e}_i &= -ke_i + ke_{i+1}, i = 1,...,n-2 \\ \dot{e}_{n-1} &= -ke_{n-1} + k_m e_n \\ \dot{e}_n &= -k_m e_n + \delta_{n+1} \\ \dot{\delta}_{n+1} &= -\frac{1}{\tau}\delta_{n+1} - \ddot{m}(t) \end{aligned} \tag{23}$$

and written in matrix form as

$$\begin{bmatrix} \dot{e} \\ \dot{\delta}_{n+1} \end{bmatrix} = (\tilde{\Lambda} \otimes I_2) \begin{bmatrix} e \\ \delta_{n+1} \end{bmatrix} - \begin{bmatrix} 0 \\ \vdots \\ 0 \\ 1 \end{bmatrix} \ddot{m}(t) \tag{24}$$

where $e=[e_1,...,e_n]^T$, $\tilde{\Lambda}=\begin{bmatrix} \tilde{\Lambda}_{11} & \tilde{\Lambda}_{12} \\ \tilde{\Lambda}_{21} & \tilde{\Lambda}_{22} \end{bmatrix}$ with

$$\tilde{\Lambda}_{11} = \begin{bmatrix} -k & k & 0 & 0 & \cdots & 0 \\ 0 & -k & k & 0 & \cdots & 0 \\ \vdots & \vdots & \vdots & \ddots & \ddots & \vdots \\ 0 & 0 & 0 & \cdots & -k & k_m \\ 0 & 0 & 0 & \cdots & 0 & -k_m \end{bmatrix} \in \Re^{n\times n},$$

$$\tilde{\Lambda}_{12} = [0,...,1]^T \in \Re^{n\times 1},$$

$$\tilde{\Lambda}_{21} = [0,...,0] \in \Re^{1\times n},$$

$$\tilde{\Lambda}_{22} = 0.$$

By using mathematical induction, it can be shown that the characteristic polynomial of matrix $\tilde{\Lambda}$ is given by $p_{\tilde{\Lambda}}(\lambda)=(\lambda+k)^{2(n-1)}(\lambda+k_m)^2+(\lambda+\frac{1}{\tau})^2$; therefore we conclude that (24) is bounded-input, bounded-state stable.

On the other hand, for the closed-loop system (1), (18), the dynamics of the errors is given by

$$\begin{aligned}
\dot{e}_i &= -ke_i + ke_{i+1} + \delta_{i+1},\ i=1,...,n-2 \\
\dot{e}_{n-1} &= -ke_{n-1} + k_m e_n + \delta_n \\
\dot{e}_n &= -k_m e_n + \delta_{n+1} \\
\dot{\delta}_i &= -\frac{1}{\tau}\left(ke_i - ke_{i+1} + \delta_i - \delta_{i+1}\right),\ i=2,...,n-2 \\
\dot{\delta}_{n-1} &= -\frac{1}{\tau}\left(ke_{n-1} - k_m e_n + \delta_{n-1} - \delta_n\right) \\
\dot{\delta}_n &= -\frac{1}{\tau}\left(k_m e_n + \delta_n - \delta_{n+1}\right) \\
\dot{\delta}_{n+1} &= -\frac{1}{\tau}\delta_{n+1} - \ddot{m}(t)
\end{aligned} \tag{25}$$

and written in matrix form as

$$\begin{bmatrix} \dot{e} \\ \dot{\delta} \end{bmatrix} = \left(\tilde{\Upsilon} \otimes I_2\right) \begin{bmatrix} e \\ \delta \end{bmatrix} - \begin{bmatrix} 0 \\ \vdots \\ 1 \end{bmatrix} \ddot{m}(t) \tag{26}$$

where $e=[e_1,...,e_n]^T$, $\delta=[\delta_2,...,\delta_n,\delta_{n+1}]^T$, $\dot{}=\begin{bmatrix} \dot{}_{11} & \dot{}_{12} \\ \dot{}_{21} & \dot{}_{22} \end{bmatrix}$, with $\dot{}_{11}=\tilde{\Lambda}_{11}$, $\dot{}_{12}$ the identity matrix of $n\times n$,

$$\tilde{\Upsilon}_{21} = \frac{1}{\tau}\begin{bmatrix} 0 & -k & k & \cdots & 0 & 0 \\ 0 & 0 & -k & \cdots & 0 & 0 \\ \vdots & \vdots & \vdots & \ddots & \ddots & \vdots \\ 0 & 0 & 0 & \cdots & -k & k_m \\ 0 & 0 & 0 & \cdots & 0 & -k_m \\ 0 & 0 & 0 & \cdots & 0 & 0 \end{bmatrix} \in \Re^{n\times n},$$

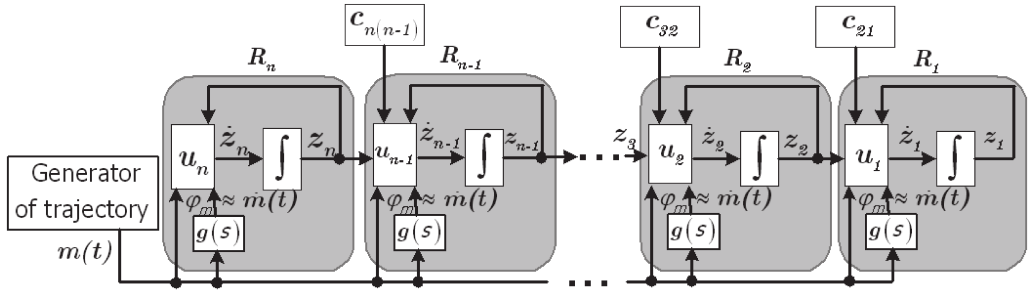

(a) Formation tracking scheme with the control law $\bar{\Gamma}_1$.

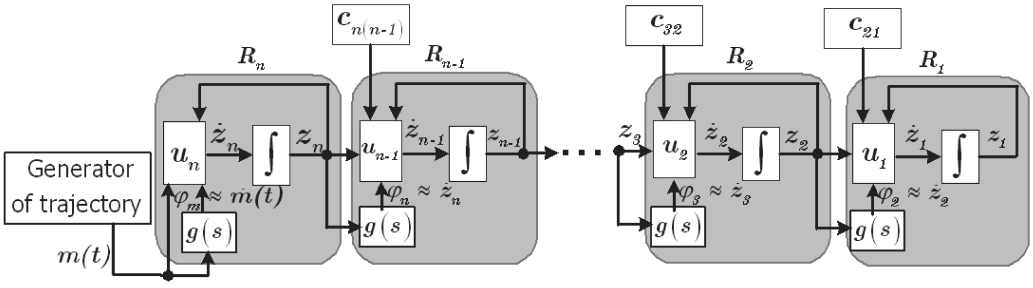

(b) Formation tracking scheme with the control law $\bar{\Gamma}_2$.

Figure 4. Formation-tracking scheme, with approximate information about the velocities of robots and the trajectory

$$\tilde{\Upsilon}_{22} = \frac{1}{\tau}\begin{bmatrix} -1 & 1 & 0 & \cdots & 0 & 0 \\ 0 & -1 & 1 & \cdots & 0 & 0 \\ \vdots & \vdots & \vdots & \ddots & \ddots & \vdots \\ 0 & 0 & 0 & \cdots & -1 & 1 \\ 0 & 0 & 0 & \cdots & 0 & -1 \end{bmatrix} \in \Re^{n\times n}.$$

Now, the characteristic polynomial of matrix $\tilde{}$ is given by $p(\lambda)=(\lambda+1)^{2n}(\lambda+k)^{2(n-1)}(\lambda+k_m)^2$; therefore we also conclude that (26) is bounded-input, bounded-state stable. In this case, observe that the eigenvalues do not depend on the value of τ.

Note that if $\ddot{m}(t)=0$, then we have a homogeneous, linear system in both cases; therefore, the solution converges exponentially to zero. Finally, the solution of the coordinate δ_{n+1}, as $t\to\infty$, is bounded by

$$|\delta_{n+1}| \le \tau |\ddot{m}(t)| \tag{27}$$

from which we can see that $|\delta_{n+1}|\to 0$ as $\tau\to 0$. □

Figure 5 shows a numerical simulation of the closed-loop systems (1), (17) and (1), (18), with $\tau=0.5$, and the same parameters and initial conditions as in Fig. 2. The error coordinates do not converge to zero, but remain bounded around zero. The transitory regime is more evident than in the case of exact information.

Analysing the effects of the gain parameter τ, define the error performance index in both cases as $\tilde{e}=\frac{1}{t_f}\int_0^{t_f}\left(\sqrt{\|e_1\|^2+\|e_2\|^2+\|e_3\|^2}\right)dt$ and $\delta=\frac{1}{t_f}\int_0^{t_f}\left(\sqrt{\|\delta_4\|^2}\right)dt$, for the control law $\bar{\Gamma}_1$ and $\delta=\frac{1}{t_f}\int_0^{t_f}\left(\sqrt{\|\delta_2\|^2+\|\delta_3\|^2+\|\delta_4\|^2}\right)dt$ for the control law $\bar{\Gamma}_2$. Table 1 shows the results for two values of τ in the previous simulation at the final time $t_f=40$. Observe the best results for the smaller values of τ, and the very similar performance of the two control laws.

	$\bar{\Gamma}_2$		τ	
$\tilde{e}$	δ	$\tilde{e}$	δ	τ
0.5	0.32	0.38	0.31	0.32
0.005	0.28	0.12	0.25	0.1

Table 1. Error-performance index with different values of $\bar{\Gamma}_1$

5. Extension of the control laws to the case of unicycle-type robots

The control laws (17) and (18) can be extended to the case of nonholonomic mobile robots. Consider the kinematic model of unicycle-type robots, as shown in Figure 6, given by

$$\begin{bmatrix}\dot{x}_i\\ \dot{y}_i\\ \dot{\theta}_i\end{bmatrix} = \begin{bmatrix}\cos\theta_i & 0\\ \sin\theta_i & 0\\ 0 & 1\end{bmatrix}\begin{bmatrix}v_i\\ w_i\end{bmatrix}, i=1,...,n, \tag{28}$$

where v_i and w_i are the linear and angular velocities, respectively, of the midpoint of the wheel's axis given by (x,y). It is known that the dynamical system (28) cannot be stabilized by application of a continuous time-invariant control law [29]. Because of this restriction, the selection of the coordinates $\alpha_i=(p_i,q_i)$, as shown in Figure 6, as a control output instead of (x,y) helps to simplify the analysis, avoiding singularities in the control law. Moreover, the position of the α_i could be the position of an actuator or the robot's center of mass. The coordinates α_i are given by

$$\alpha_i = \begin{bmatrix}p_i\\ q_i\end{bmatrix} = \begin{bmatrix}x_i + l\cos\theta_i\\ y_i + l\sin\theta_i\end{bmatrix}, i=1,...,n, \tag{29}$$

and their dynamics can be obtained as

$$\dot{\alpha}_i = \underbrace{\begin{bmatrix}\cos\theta_i & -l\sin\theta_i\\ \sin\theta_i & l\cos\theta_i\end{bmatrix}}_{A_i(\theta_i)}\begin{bmatrix}v_i\\ w_i\end{bmatrix}, i=1,...,n, \tag{30}$$

where $A_i(\theta_i)$ is the so-called decoupling matrix of the robot R_i. Note that $\det(A_i(\theta_i))=l\neq 0$. Therefore, it is possible to design a control strategy in order to move α_i to a desired location using the control law $[v_i,w_i]^T=A_i^{-1}(\theta_i)f_i, i=1,...,n$, where functions f_i are the desired dynamics of the coordinates α_i.

Thus, extending the previous results to the case of point robots, the control laws with exact velocities given in (4)-(5), or the control laws with approximate velocities expressed in (17)-(18), could be rewritten for unicycle robots by

$$\begin{bmatrix}v_i\\ w_i\end{bmatrix} = \frac{1}{2}A_i^{-1}(\theta_i)(\bar{u}_i),\ i=1,...n \tag{31}$$

where $\bar{u}_i$ are identical functions of the control laws u_i as defined in (4)-(5) and (17)-(18), depending on the coordinates αi. Note that the dynamics of the coordinates α_i in the closed-loop system (29)-(31) are reduced to $\alpha_i=\bar{u}_i$, $i=1,...,n$. Therefore, the analysis of the formation tracking becomes in the case of holonomic robots studied in Sections 3 and 4. Note that these input-output linearizations leave the orientation angles θ_i in an uncontrolled state.

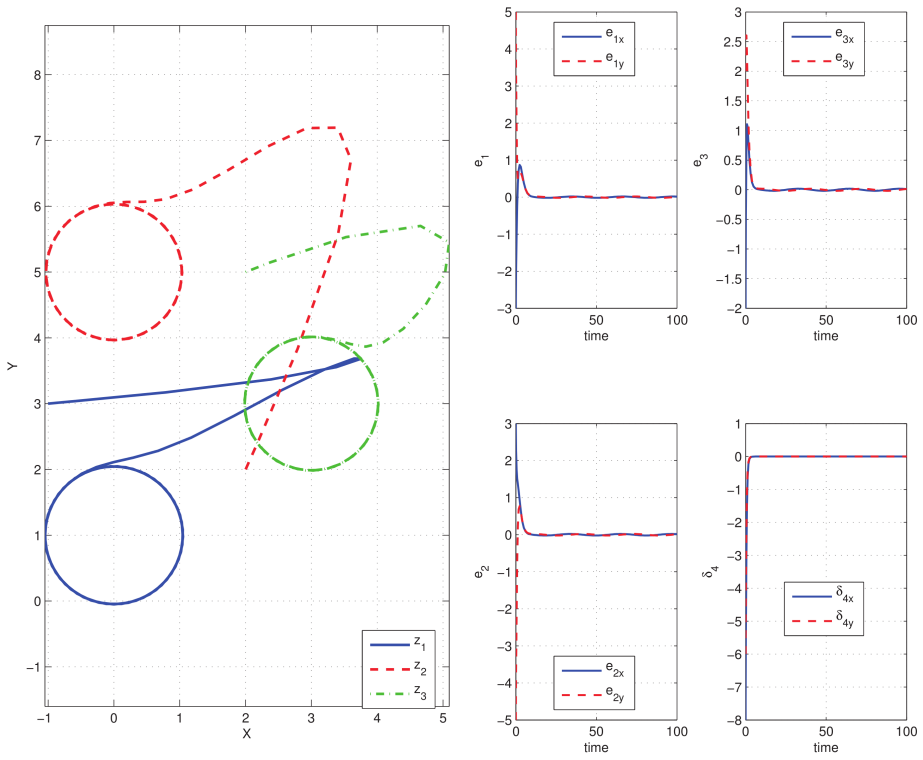

(a) Control law $\bar{\Gamma}_1$ with $\tau = 0.5$

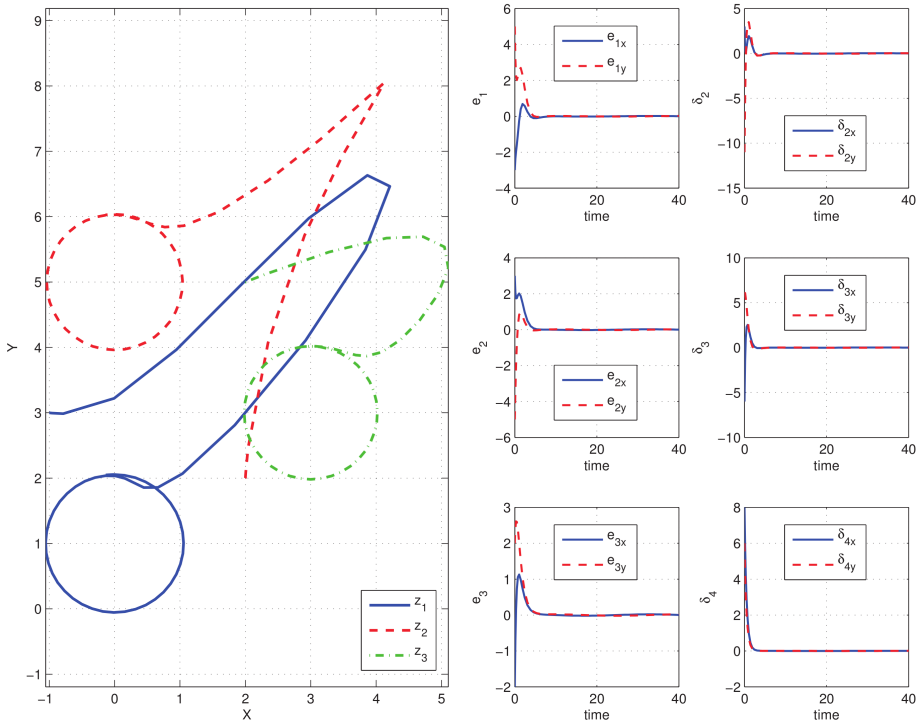

(b) Control law $\bar{\Gamma}_2$ with $\tau = 0.5$

Figure 5. IRobot Create

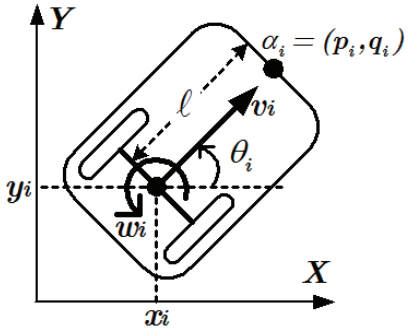

Figure 6. Simulation of formation tracking using approximate velocities

Figure 7. Kinematic model of unicycles

6. Experimental work

The control strategies were implemented using an experimental set-up consisting of three unicycle-type robots manufactured by IRobot, the model Create, and a vision system comprising a monochrome camera Genie HM-1024 with an Ethernet communication, developed by Teledyne Dalsa. The camera captures the position of two white circle marks placed on top of every robot, as shown in Fig. 5, indicating the coordinates (x_i, y_i) and α_i. The camera is installed at a height of 2.5m and configured to work at 117 frames per second. Therefore, the sampling period is given by 8 milliseconds and the resolution of the camera is given by 1024×768 pixels which produces a position resolution of 3mm^2 per pixel. Note that both the workspace and the robots are covered in black in order to highlight the white markings.

Using the white marks, the position and orientation of every robot is calculated using a Core i5 PC with 4GB RAM. The same computer subsequently evaluates the control laws and generates the control signals u_i and w_i for every robot, which are transformed into the desired angular velocities for the robot wheels, by

$$wr_i = \frac{v_i}{r} + \frac{L}{2r} w_i, \; i = 1,...n \tag{32}$$

$$wl_i = \frac{v_i}{r} - \frac{L}{2r} w_i, \; i = 1,...n \tag{33}$$

where wr_i and wl_i are the right and left wheel of each robot, respectively, L =0.25m is the distance between two wheels and r=0.03m is the radius of the wheels. Finally, the desired angular velocities are sent via a wireless Bluetooth transmitter to every robot. The image processing and the control law were developed in a software application using the real-time programming of Matlab *R*2013*a*.

Note that the experimental set-up becomes a flexible platform for emulating different formation-tracking systems, from centralized to decentralized schemes, by selecting the adequate information obtained from the vision system to be used in the local control laws of each robot.

To complement the control laws, a reactive secondary control law for the avoidance of inter-robot collision was programmed into the experiments. Although the prevention of possible collisions was achieved using a simple reactive control law, in the experiments, none of the robots were in danger of collision due to their initial conditions. The analysis of non-collision in formation tracking is not studied in this paper and will be addressed in further research.

6.1 Experiments with exact velocities

Figure 8 shows an experiment of the control law Γ_1 given in (4) using the exact information of the derivative of $m(t)$, with n=3, k=1, k_m=1 and ℓ=0.15m. The marching path is the circle given (in metres) by $m(t)=\left[0.5+0.4\cos\left(\frac{2\pi}{40}t\right), 0.5+0.4\sin\left(\frac{2\pi}{40}t\right)\right]$. The vectors of the relative positions are $c_{21}=c_{32}=[0.6m,0]$ (a straight-line shaped formation). The initial conditions, also given in metres and radians, are given by $[x_1,y_1,\theta_1]=[2.23,0.68,1.56]$, $[x_2,y_2,\theta_2]=[1.69,0.68,1.50]$ and $[x_3,y_3,\theta_3]=[1.14,0.66,1.65]$. The trajectories of the coordinates α_i that are recorded by the vision system are presented in Figure 8(a). The leader robot R_3 converges to the desired marching path whereas the follower robots converge to the desired formation. The evolution of x_i, y_i and θ_i is depicted in Figure 8(b). Note that the experimental results are very close to the simulation signals. Finally, the control outputs v_i and w_i are shown in Figure 8(c).

The second experiment is given in Figure 9, which is now dedicated to the control law Γ_2 given in (5) using the exact information of the robots' velocities. The value of the control gains k and k_m are similar to the ones used in the previous case. Now the robots are formed in a triangular shape, given by the vectors $c_{21}=[0.6,0.6]$ and $c_{32}=[0.6,-0.6]$. The initial conditions are $[x_1,y_1,\theta_1]=[2.26,0.70,1.68]$, $[x_2,y_2,\theta_2]=[2.03,1.45,2.85]$ and $[x_3,y_3,\theta_3]=[1.03,0.65,0.68]$. The trajectories of the coordinates α_i that are recorded by the vision system are presented in Figure 9(a). The evolution of x_i, y_i and θ_i is depicted in Figure 9(b). The control outputs v_i and w_i are shown in Figure 9(c). Similar to the previous

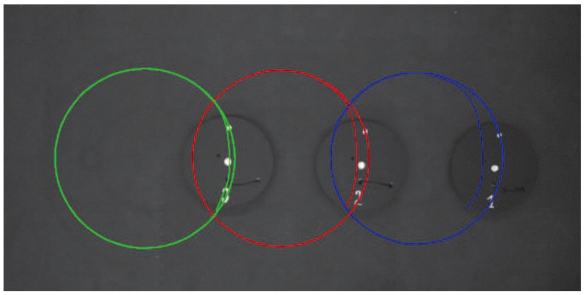

(a) Position of the robots in the workspace.

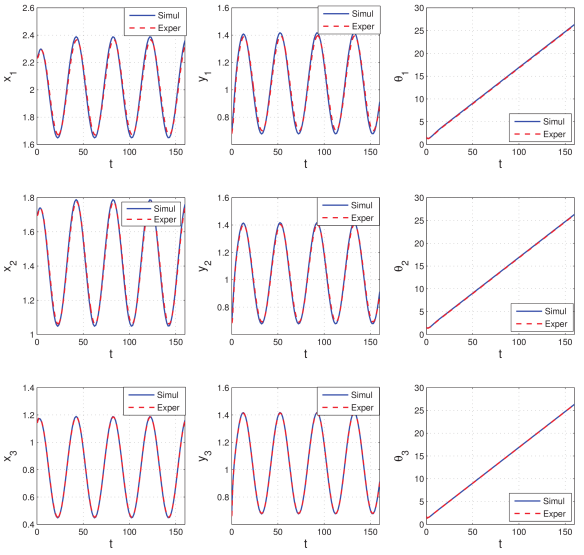

(b) Coordinates x_i, y_i, θ_i.

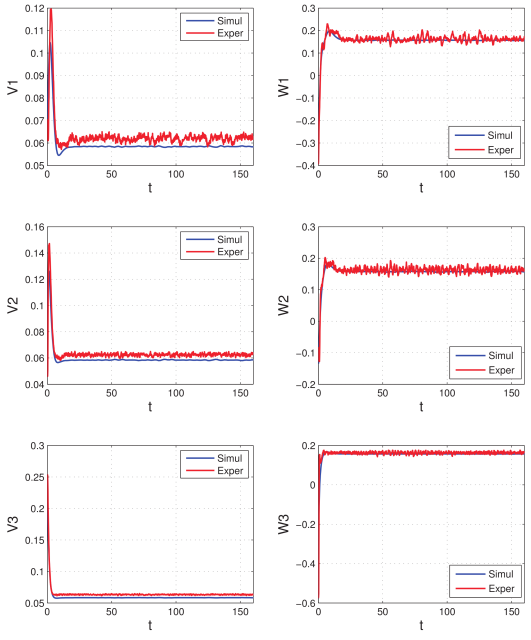

(c) Linear and angular velocities

Figure 8. Experiment 1 using the control law Γ_1

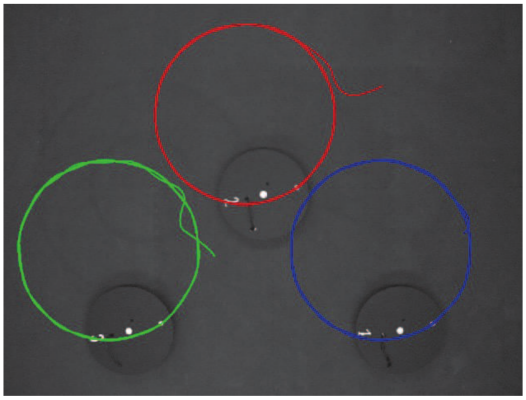

(a) Position of the robots in the workspace.

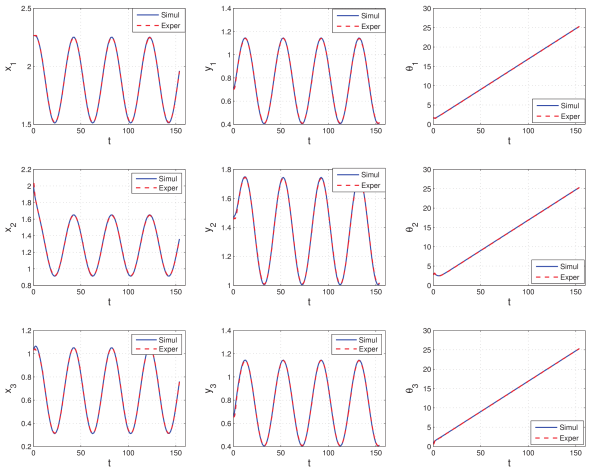

(b) Coordinates x_i, y_i, θ_i.

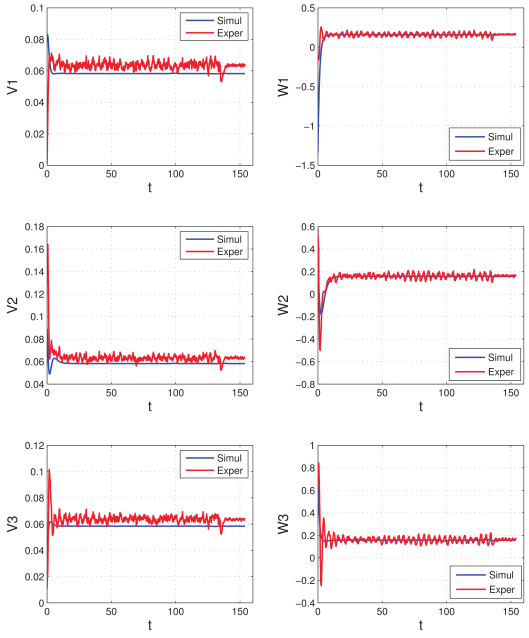

(c) Linear and angular velocities

Figure 9. Experiment 2 using the control law x_i

case, the graphs show a good performance of the control law, in which the robots converge to the desired formation tracking and the experimental results are close to the numerical simulation.

In both experiments, the orientation angles converge to the same value although they are not controlled by the control laws. In addition, note that the linear and angular velocities

shown in Figures 8(c) and 9(c) converge to a positive value; therefore, the robots after the transitory regime, continue to move in an antoclockwise direction while facing the front. It is shown in Figures 8(b) and 9(b) where the trajectories of coordinates y_i and Γ_2, respectively, describe the parametric functions of the circumference, and that the orientation angles are positive and increasing.

The quantization error is considered to be sufficiently small for this experiment, due to the precision of the camera and the insignificance of its influence. This can be seen in Figures 8 and 9, where the results show a ripple in the order of the instrument's resolution.

6.2 Experiments with approximate velocities

Figure 10 shows an experiment 3 using the control law $\bar{\Gamma}_1$ with $\tau=0.5$. The marching path and desired vector of the positions are similar to those of the experiment 1 shown in Figure 8. Now, the initial conditions are $[x_1,y_1,\theta_1]=[2.3679,1.1637,1.8659]$, $[x_2,y_2,\theta_2]=[1.7655,1.1773,1.9130]$ and $[x_3,y_3,\theta_3]=[1.1632,1.1920,1.9660]$. The trajectories of the coordinates α_i, which are recorded by the vision system, are presented in Figure 10(a). The evolutions of x_i, y_i and θ_i are depicted in Figure 10(b). The control outputs v_i and w_i are shown in Figure 10(c).

Finally, the fourth experiment is given in Figure 11, using the control law $\bar{\Gamma}_2$ with $\tau=0.5$. The marching paths and desired vectors of the positions are similar to those of Experiment 2 as shown in Figure 9. The initial conditions are $[x_1,y_1,\theta_1]=[1.8747,0.7022,1.3280]$, $[x_2,y_2,\theta_2]=[1.3245,1.3362,1.6792]$ and $[x_3,y_3,\theta_3]=[0.6352,0.6170,1.4002]$. The trajectories of the coordinates α_i recorded by the vision system are presented in Figure 11(a). The evolution of x_i, y_i and θ_i is depicted in Figure 11(b). The control outputs v_i and w_i are shown in Figure 11(c).

Note that the trajectories in Experiments 3 and 4 are modified due to the approximations of the velocities and the performance of the robots deteriorating with respect to the ideal case. The transient response of the control inputs, as shown in Figures 10(c) and 11(c), exhibits a larger overshoot with respect to the control inputs of Experiments 1 and 2, as presented in Figures 8(c) and 9(c), respectively, with the worst being Experiment 4. Similar to Experiments 1 and 2, the linear and angular velocities converge to a positive value; therefore, the robots continue to move in an antoclockwise direction while facing the front, which is verified by the trajectories depicted in Figures 10(b) and 11(b), respectively.

According to the main result detailed in Section 4, the errors remain oscillatory around zero. These effects are shown in Figure 12 for Experiments 3 and 4, respectively. Note that due to propagation of the inexact measures of velocities along the chain of robots, the behaviour of the errors worsen in robots that move away from the leader. Thus, the robot R_1 exhibits the worst performance in the formation tracking.

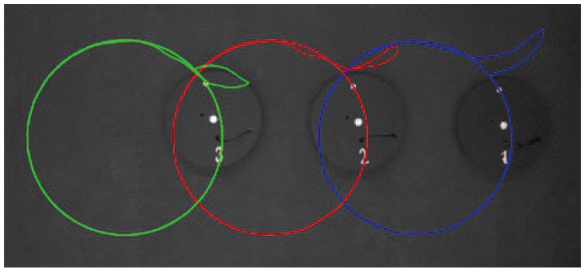

(a) Position of the robots in the workspace.

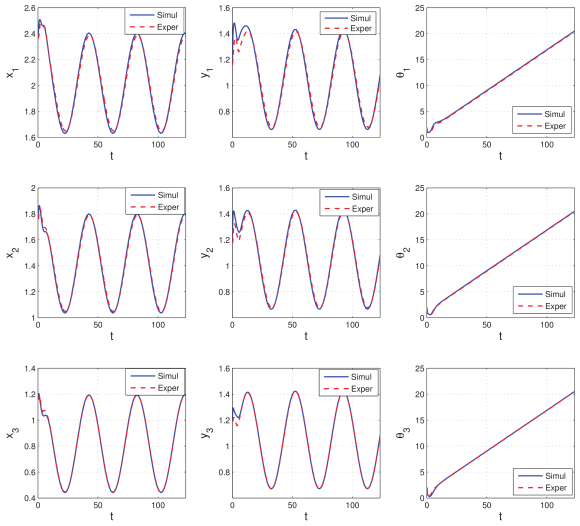

(b) Coordinates x_i, y_i, θ_i.

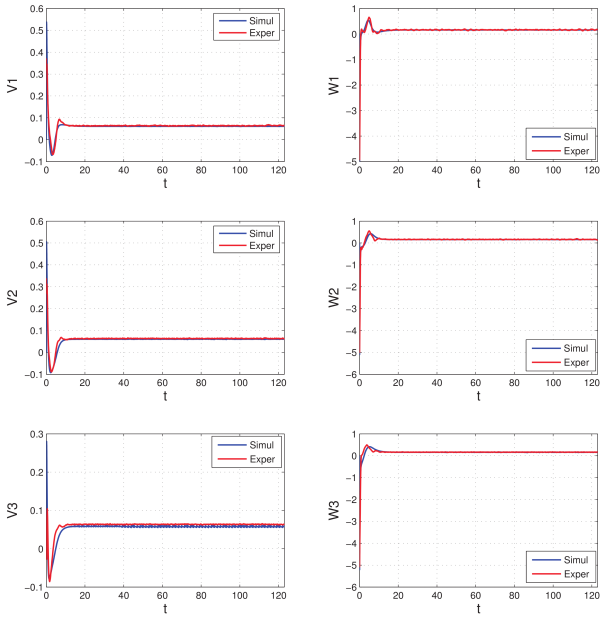

(c) Linear and angular velocities

Figure 10. Experiment 3 using the control law $\bar{\Gamma}_1$ and $\tau=0.5$

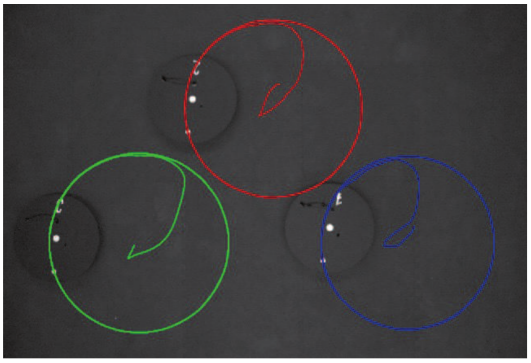

(a) Position of the robots in the workspace.

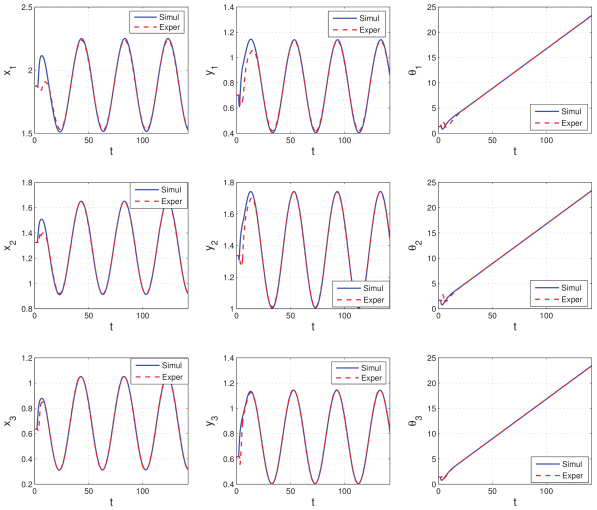

(b) Coordinates x_i, y_i, θ_i.

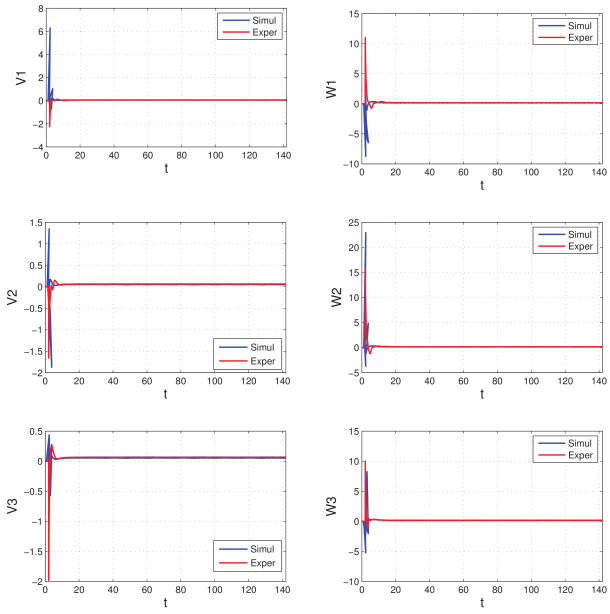

(c) Linear and angular velocities

Figure 11. Experiment 4 using the control law $\bar{\Gamma}_2$ and $\tau = 0.5$

7. Conclusion

This paper shows that, assuming perfect knowledge about the positions and velocities of the robots and the marching path, it is possible to guarantee the preservation of a rigid formation and the group trajectory tracking of the robots. However, during a decentralized formation tracking, the robots measure only positions and the velocities must be approximated. This paper incorporates the analysis of the variables of approximate velocities within the closed-loop systems, and some conditions are determined in order to ensure that the errors are bounded. The desired outcome occurs if the trajectory is sufficiently smooth and the bound of the errors' performance improves when the bandwidth approximation increases for the velocities, recovering the ideal case in the limit. The control laws were extended for the case of unicycle-type robots with numerical simulations and real-time experiments. In further research, the analysis

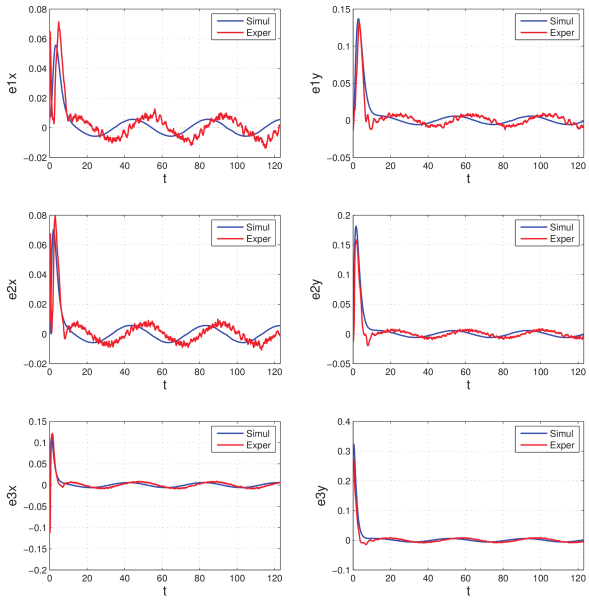

(a) Experiment 3 with the control law $\bar{\Gamma}_1$

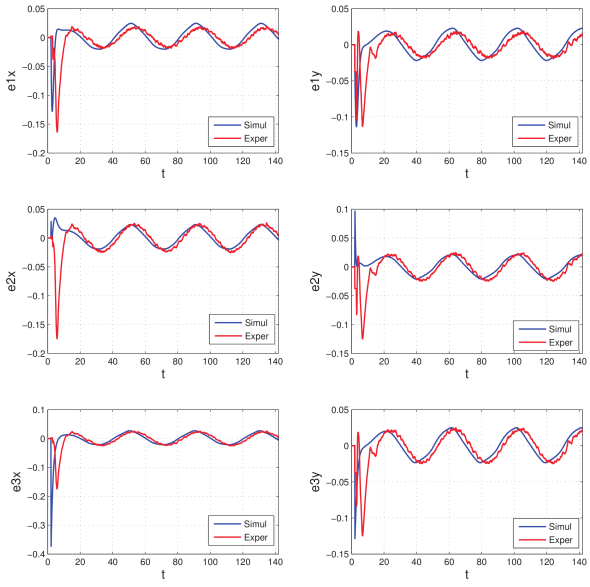

(b) Experiment 4 with the control law $\bar{\Gamma}_2$

Figure 12. Graphics of errors using approximate velocities

of control strategies with other formation-tracking topologies and collision avoidance applied to different nonholonomic mobile robots will be studied.

8. Acknowledgements

The authors kindly acknowledge the financial support of the Universidad Iberoamericana and the Universidad Católica del Uruguay.

9. References

[1] T. Arai, E. Pagello, and L. E. Parker. Guest editorial advances in multirobot systems. *IEEE Transactions on Robotics and Automation*, Vol. 18(No. 5):655–661, October 2002.

[2] Y. Q. Chen and Z. Wang. Formation control: A review and a new consideration. In *International Conference on Intelligent Robots and Systems*, pages 3181–3186, Edmonton, Canada, August 2005. IEEE/RSJ.

[3] C. Reynolds. Flocks, birds, and schools: A distributed behavioral model. *Computer Graphics*, Vol. 21(No. 1):25–34, 1987.

[4] K.D. Do. Formation tracking control of unicycle-type mobile robots. In *International Conference on Robotics and Automation*, pages 2391–2396, Roma, Italy, April 2007. IEEE.

[5] J. Ghommam, H. Mehrjerdi, M. Saad, and F. Mnif. Formation path following control of unicycle-type mobile robots. *Robotics and Autonomous Systems*, Vol. 58(No. 5):727–736, 2010.

[6] E.G. Hernandez-Martinez and E. Aranda-Bricaire. Marching control of unicycles based on the leader-followers scheme. In *35th Annual Conference of the IEEE Industrial Electronics Society*, pages 2265–2270, Porto, Portugal, November 2009. IEEE.

[7] A. Regmi, R. Sandoval, R. Byrne, H. Tanner, and C.T. Abdallah. Experimental implementation of flocking algorithms in wheeled mobile robots. In *American Control Conference*, pages 4917–4922, Portland, USA, June 2005. IEEE.

[8] D. Kostic, S. Adinandra, J. Caarls, N. van de Wouw, and H. Nijmeijer. Saturated control of time-varying formations and trajectory tracking for unicycle multi-agent systems. In *Conference on Decision and Control*, pages 4054–4059, Atlanta, USA, December 2010. IEEE.

[9] H.G. Tanner, V. Kumar, and G.J. Pappas. Leader-to-formation stability. *IEEE Transactions on Robotics and Automation*, Vol. 20(No. 3):443–455, June 2004.

[10] F. Belkhouche and B. Belkhouche. Modelling and controlling a robotic convoy using guidance laws strategies. *IEEE Transactions on Systems, Man and Cybernetics, Part B*, Vol. 35(No. 4):813–825, August 2005.

[11] M. Porfiri, D.G. Roberson, and D.J. Stilwell. Tracking and formation control of multiple autonomous agents: A two-level consensus approach. *Automatica*, Vol. 43(No. 8):1318–1328, August 2007.

[12] J. Ghommam, H. Mehrjerdi, and M. Saad. Robust formation control without velocity measurement of the leader robot. *Control Engineering Practice*, 21:1143–1156, 2013.

[13] L. Consolini, F. Morbidi, D. Prattichizzo, and M. Tosques. Leader-follower formation control of nonholonomic mobile robots with input constraints. *Automatica*, Vol. 44(No. 5):1343–1349, May 2008.

[14] K. Choi, S.J. Yoo, J.B. Park, and Y.H. Choi. Adaptive formation control in absence of leader's velocity information. *IET Control Theory and Applications*, Vol. 4(No. 4):521–528, April 2010.

[15] K.D. Do. Output-feedback formation tracking control of unicycle-type mobile robots with limited sensing ranges. *Robotics and Autonomous Systems*, Vol. 44(No. 1):34–47, January 2009.

[16] Z. Peng, D. Wang, and X. Hu. Robust adaptive formation control of underactuated autonomous surface vehicles with uncertain dynamics. *IET Control Theory and Applications*, Vol. 5(No. 12):1378–1387, January 2011.

[17] B. Lu, F. Chen, and L. Weiyao. Distributed tracking of a rigid formation for multi-agent systems. In *Proceedings of the 33rd Chinese Control Conference*, pages 1288–1292, Nanjing, China, Jul 2014.

[18] Z. Weihua and T.H. Go. Robust cooperative leader-follower formation flight control. In *11th International Conference on Control Automation Robotics and Vision*, pages 275–280, Singapore, December 2010. IEEE.

[19] H. Bai, M. Arcak, and J.T. Wen. Adaptive design for reference velocity recovery in motion coordination. *Systems and control letters*, Vol. 57(No. 1):602–610, August 2008.

[20] H. Bai, M. Arcak, and J.T. Wen. Adaptive motion coordination: using relative velocity information to track a reference velocity. *Automatica*, Vol. 45(No. 4): 1020–1025, April 2009.

[21] T. Dierks, B. Brenner, and S. Jagannathan. Neural network-based optimal control of mobile robot formations with reduced information exchange. *IEEE Transactions on Control Systems Technology*, 21(4):1407–1415, 2013.

[22] W. Wang, J. Huang, C. Wen, and H. Fan. Distributed adaptive control for consensus tracking with application to formation control of nonholonomic mobile robots. *Automatica*, 50:1254–1263, 2014.

[23] W. Dong. Tracking control of multiple wheeled mobile robots with limited information of a desired

trajectory. *IEEE Transactions on Robotics*, Vol. 28(No. 1):262–268, April 2012.

[24] W. Ren and N. Sorensen. Distributed coordination architecture for multi-robot formation control. *Robotics and Autonomous Systems*, Vol. 56(No. 4): 324–333, April 2008.

[25] R. Haghighi and C.C. Cheah. Distributed shape formation of multi-agent systems. In *International Conference on Control, Automation, Robotics and Vision*, pages 1466–1471, Guangzhou, China, December 2012. IEEE.

[26] Q. Hu and J. Zhang. Relative position finite-time coordinated tracking control of spacecraft formation without velocity measurements. *ISA Transactions*, 54:60–74, 2015.

[27] E.G. Hernandez-Martinez and E. Aranda-Bricaire. Trajectory tracking for groups of unicycles with convergence of the orientation angles. In *Conference on Decision and Control*, pages 6323–6328, Atlanta, USA, December 2010. IEEE.

[28] H. Yamaguchi. A distributed motion coordination strategy for multiple nonholonomic mobile robots in cooperative hunting operations. *Robotics and Autonomous Systems*, Vol. 43(No. 1):257–282, April 2003.

[29] R. Brockett, R.S. Millman, and H. J. Sussmann. *Asymptotic Stability and Feedback Stabilization*. Birkhauser, Massachusetts, 1983.